RESEARCH

2007-01

Use of Ground Penetrating Radar to Evaluate Minnesota Roads

Mn ROAD
Office of Materials

LRRB
LOCAL ROAD RESEARCH BOARD

Take the steps... Research...Knowledge...Innovative Solutions!

Transportation Research

Technical Report Documentation Page

1. Report No. MN/RC-2007-01	2.	3. Recipients Accession No.	
4. Title and Subtitle Use of Ground Penetrating Radar to Evaluate Minnesota Roads		5. Report Date January 2007	
		6.	
7. Author(s) Marc C. Loken		8. Performing Organization Report No. .	
9. Performing Organization Name and Address Minnesota Department of Transporation Office of Materials 1400 Gervais Avenue Maplewood, MN 55109		10. Project/Task/Work Unit No.	
		11. Contract (C) or Grant (G) No.	
12. Sponsoring Organization Name and Address Minnesota Department of Transportation 395 John Ireland Boulevard Mail Stop 330 St. Paul, Minnesota 55155		13. Type of Report and Period Covered Final Report 2006	
		14. Sponsoring Agency Code	
15. Supplementary Notes ttp://www.lrrb.org/PDF/200701.pdf			
16. Abstract (Limit: 200 words) The Minnesota Local Road Research Board (LRRB) funded a project to evaluate the usefulness of ground-penetrating radar (GPR) in evaluating Minnesota roads. A literature search was first performed to review the applications of ground-penetrating radar (GPR) to highway applications. These applications include calculating layer thickness, estimating asphalt density, determining aggregate base moisture content, identifying stripping within asphalt layers, detecting air voids and vertical cracks, identifying subsurface anomalies, and analyzing rutting mechanisms. The relative accuracy of using GPR as opposed to traditional field tests was assessed. A simple laboratory calibration was performed to estimate the thickness of a concrete slab to within 10%. Finally, a sensitivity study was performed to determine the dependence of various output parameters (minimum layer thickness, maximum depth of penetration, horizontal resolution, reflection coefficients, layer thickness, and air void thickness) on input parameters (antenna frequency and dielectric constant). GPR was successful in identifying total asphalt thickness on CSAH 61 in Pine County, and moderately successful in determining base thickness and identifying the underlying, original concrete roadway in select locations. The surveys were not successful in differentiating asphalt course thicknesses. The surveys also identified potential regions of stripping. GPR was not successful in locating near-surface bedrock or peat deposits on CSAH 48 in St. Louis County, because of the presence of a geo-textile membrane.			
17. Document Analysis/Descriptors Key words: Ground penetrating radar, layer thickness, void detection, stripping, base moisture content, asphalt density		18. Availability Statement No restrictions. Document available from: National Technical Information Services, Springfield, Virginia 22161	
19. Security Class (this report) Unclassified	20. Security Class (this page) Unclassified	21. No. of Pages 45	22. Price

Use of Ground Penetrating Radar to Evaluate Minnesota Roads

Final Report

Prepared by:

Marc Loken

Senior Engineer
Minnesota Department of Transportation
Office of Materials
1400 Gervais Avenue
Maplewood, MN 55109-2044

January 2007

Published by:

Minnesota Department of Transportation
Research Services Section
395 John Ireland Boulevard, MS 330
St. Paul, Minnesota 55155-1899

Table of Contents

List of Figures

List of Tables

Executive Summary

The Minnesota Local Road Research Board (LRRB) funded a project to evaluate the usefulness of ground-penetrating radar (GPR) in evaluating Minnesota roads. A Technical Advisory Panel (TAP) was set up to oversee this project and they identified two test sites (CSAH 61 in Pine County and CSAH 48 in St. Louis County) for this project. The first test site is located in Pine County and is a ten-mile stretch of CSAH 61 that runs north from the Snake River in Pine City to Interstate 35 at the junction of TH23. This section of road has a history of numerous thin asphalt overlays. GPR may be useful in delineating the different overlays that have been constructed over the years. In addition, if stripping can be detected, it would prove to be very useful in planning rehabilitation of the roadway. The second test site is CSAH-48, or LaVaque Road as it is locally known in St. Louis County. This 5-mile stretch of highway just west of Duluth is a good GPR candidate site because of its potential to locate near-surface bedrock and peat deposits, both of which are common in northern Minnesota.

A literature search was first performed to review the applications of ground-penetrating radar (GPR) to highway applications. These applications include calculating layer thickness, estimating asphalt density, determining aggregate base moisture content, identifying stripping within asphalt layers, detecting air voids and vertical cracks, identifying subsurface anomalies, and analyzing rutting mechanisms. The relative accuracy of using GPR as opposed to traditional field tests was assessed. A simple laboratory calibration was performed to estimate the thickness of a concrete slab within to 10%. Finally, a sensitivity study was performed to determine the dependence of various output parameters (minimum layer thickness, maximum depth of penetration, horizontal resolution, reflection coefficients, layer thickness, and air void thickness) on input parameters (antenna frequency and dielectric constant).

GPR was successful in identifying total asphalt thickness on CSAH 61 in Pine County, and moderately successful in determining base thickness and identifying the underlying, original concrete roadway in select locations. The surveys were not successful in differentiating asphalt course thicknesses. The surveys also identified potential regions of stripping.

GPR was not successful in locating near-surface bedrock or peat deposits on CSAH 48 in St. Louis County, because of the presence of a geo-textile membrane.

1. Introduction

Ground penetrating radar (GPR) is a noninvasive, continuous, high-speed tool that has been used to map subsurface conditions in a wide variety of applications. Many of these applications are well suited for evaluation of highway systems. GPR is basically a subsurface "anomaly" detector, as such it will map changes in the underground profile due to contrasts in the electromagnetic conductivity across material interfaces.

GPR technology has a relative recent history. Radar was developed and used during World War II to detect and track metal objects, such as aircraft or ships. The first radar specifically designed to penetrate the ground was developed at MIT in the late 1960's for the U.S. military to find shallow tunnels in Vietnam. In 1970 the first commercial company was established to manufacture and sell GPR equipment and services. In 1974 the first GPR patent was issued. Since that time the GPR technology has boomed, paralleling the technological advances in the computer industry.

Local road authorities are faced with unknowns when planning projects. The objective of this project is to determine if ground-penetrating radar (GPR) survey equipment and techniques can be used to accurately detect subsurface defects, distresses, and other features in Minnesota pavements. This research will lead to an understanding of the relative advantages and disadvantages of GPR as applied to pavements, materials, and conditions unique to the state of Minnesota. In addition it will provide practical experience in GPR data processing, interpretation procedures, and associated software.

A Technical Advisory Panel (TAP) has been selected to overview this project. The members of this panel include:

- John Stieben, Pine County Engineer, Technical Liaison (TL);
- James Klessig, Mn/DOT, Administrative Liaison (AL);
- Marc Loken, Mn/DOT, Principal Investigator (PI);
- Mike Robinson, Mn/DOT, Technical Advisor (TA);
- Steve Oakey, Mn/DOT, Technical Advisor (TA);
- Joel Ulring, St. Louis County Engineer, Technical Advisor (TA);
- Dave Van Deusen, Mn/DOT, Technical Advisor (TA);
- Shongtao Dai, Mn/DOT, Technical Advisor (TA);
- Greg Johnson, Mn/DOT, Technical Advisor (TA).

The TAP identified two sites for GPR investigation, State Highway (CSAH) 61 in Pine County and County State Aid Highway (CSAH) 48 in St. Louis County. John Stieben identified a 10-mile stretch of CSAH-61 in Pine County. The road section runs from the Snake River in Pine City north to Interstate 35 at Mission Creek. This section of road has a history of asphalt overlays. GPR may be useful in delineating the different overlays that have been constructed over the years. In addition, if stripping can be detected, it would prove to be very useful in planning rehabilitation of the roadways. Joel Ulring identified CSAH-48, or LaVaque Rd as it is locally known, as a good GPR candidate site, because of its potential to locate near-surface bedrock and peat deposits, both of which are common in northern Minnesota. This report summarizes two GPR surveys performed on CSAH-48. The first stretch of this highway runs north from the city of Proctor to the intersection of Morris Thomas Road, a distance of approximately 3 miles. GPR could be useful in locating the depth to bedrock and identifying peat deposits, which both underlie the constructed roadway, sometimes at fairly shallow depths.

In addition, detailed records of recent soil borings exist at this site, which could be used to validate the GPR surveys.

The remainder of this report is divided into five sections. The mathematical principles of GPR and a literature review are briefly discussed in the next section. Section 3 summarizes the calibration and sensitivity studies. The results of the GPR surveys of CSAH 61 are presented in Section 4. Section 5 contains the GPR surveys of CSAH 48. A short summary concludes the report. The cited references are listed in the bibliography. A series of appendices contains detailed results from this study.

2. Task 1: Literature Review

2.1 Mathematical Principles

GPR operates by transmitting short pulses of electromagnetic energy downward into the ground. The reflected images of these pulses are analyzed using one-dimensional electromagnetic wave propagation theory. These pulses are reflected back to the antenna with amplitudes and arrival times that are related to the electrical conductivities (equivalently, dielectric constants) of the material layers. Across the interfaces, part of the energy is reflected and part is absorbed, depending on the dielectric contrast of the materials. The observed peaks in amplitude (in their order of occurrence) represent the antenna end reflection (A_0), the surface (pavement) reflection (A_1), the base reflection (A_2), and the subgrade reflection (A_3), respectively. The time interval (t_1) between peaks A_1 and A_2 represents the two-way travel time through the pavement layer. Similarly, the time interval ()t_2) between peaks A_2 and A_3 represents the two-way travel time through the base layer. The thickness of each layer (h_i) can be calculated as:

$$h_i = v_i \, t_i / 2 \qquad (1)$$

where: v_i = propagation velocity through each layer.

The propagation velocity is related to the electromagnetic behavior of the material:

$$v_i = c / \sqrt{\varepsilon_i} \qquad (2)$$

where: ε_i = dielectric constant of each layer

c = speed of light in air
= 11.8 in/ns (.30 m/ns)

The dielectric constant of the pavement layer (ε_1) is calculated as:

$$\sqrt{\varepsilon_1} = (1 + \rho_1) / (1 - \rho_1) \qquad (3)$$

where: $\rho_1 = A_1/A_m$

A_1 = the amplitude of the GPR wave from the pavement surface
A_m = the amplitude of the GPR wave from a metal plate (100% reflection)

Similarly, the dielectric constant for the base layer (ε_2) is calculated as:

$$\sqrt{\varepsilon_2} = \sqrt{\varepsilon_1} \, (1 - \rho_1^2 + \rho_2) / (1 - \rho_1^2 - \rho_2) \qquad (4)$$

where: $\rho_2 = A_2/A_m$

A_2 = the amplitude of the GPR wave from the surface of the base layer

Ranges in dielectric constants for typical pavement materials are given in the following table.

Table 2-1 Dielectric Constants and Propagation Velocities of Pavement Materials

Material	Dielectric Constant (-)	Propagation Velocity (m/s)
Air	1	.30
Ice (Frozen soil)	4	.15
Granite	9	0.10
Limestone	6	0.12
Sandstone	4	0.15
Dry sand	4 to 6	0.12 to 0.15
Wet sand	30	0.055
Dry clay	8	0.11
Wet clay	33	0.052
Asphalt	3 to 6	0.12 to 0.17
Concrete	9 to 12	0.087 to 0.10
Water	81	0.033
Metal	8	0

2.2 Applications

GPR has been used successfully in a variety of highway applications, including: (1) measuring layer thickness of asphalt pavements, concrete pavements, and granular base layers; (2) estimating asphalt densities; (3) determining moisture content of base materials; (4) identifying stripping zones in asphalt layers; (5) detecting air-filled and water-filled voids; (6) locating subsurface vertical cracks; (7) locating subsurface "anomalies" including buried objects, peat deposits, and near-surface bedrock; and analyzing rutting mechanisms. These applications are discussed separately in the following subsections.

2.2.1 Layer Thickness

Existing pavement layer thickness measurement methods include coring and test pit excavations. These direct methods are both time consuming and expensive. Furthermore, they only provide information at the test location, i.e., they are point measurements. In contrast, GPR surveys are much less time consuming and provide a continuous description of the road structure. Thus, determination of pavement layer thickness is one of the more successful applications of GPR. The American Society for Testing and Materials (ASTM) Standard D 4748-87 [ASTM Standard Designation: D4748-87, 1987] presents detailed procedures for determining the thickness of pavements using GPR.

Pavement thickness evaluation is based on the measurement of the time difference between layer reflections and knowing the propagation velocity (or equivalently, the dielectric constant) within each layer. The reflections from the interfaces must be strong enough to be interpreted and tracked for reasonably consistent results. Experience has shown that GPR works well on flexible pavements (asphalt) where there is a strong dielectric contrast between layers, but may be less effective on rigid pavements (concrete) where the presence of moisture tends to attenuate the radar signal, or where the contrast between layers is minimal such as between concrete and granular base materials.

Despite limitations associated with weak signals and material dielectric uncertainties, the advantages of determining thickness with GPR are considerable, since it is a nondestructive, continuous, and high-speed field test.

Using GPR, layer thicknesses can be estimated in one of two ways, (1) using blind estimates and (2) using ground truth measurements. Blind estimates involve using Equations 3 and 1 alone to estimate the asphalt dielectric and thickness. Ground truth measurements involve adjusting the dielectric constant to match the predicted thickness at locations where core are taken. Obviously the predictions become more accurate in comparison with ground truth measurements.

Nearly one-half of the state DOT's have implemented some kind of GPR system into their pavement engineering research programs. The most successful application of this research is in pavement thickness evaluation, and several states have adopted GPR into their routine pavement evaluation programs. The results of these studies are summarized here.

Texas Studies [Maser and Scullion, 1992; Maser, 1990; and Maser, 1992c]

Four asphalt pavement sites near College Station, Texas were evaluated in this study to determine asphalt and base thickness. Each test site was 1500 ft long, and four surveys were carried out at each site at various collection speeds ranging from 5 to 40 mph. Coring was used to measure asphalt thickness at several locations along the test sections. The asphalt thickness varied from 2 to 10 inches at these locations. A penetrometer and visual observation in the dry coreholes were used to determine the base thicknesses. The base thickness varied from 5 to 12 inches. The accuracy of the radar predictions for asphalt thickness was within 0.32 inches (4%) using the radar data alone, (blind estimates) and within 0.11 inches (1.4%) when one calibration core was used per site (ground truth). The accuracy of the radar predictions for the base thickness was within 1 inch (17%).

Kansas Study [Roddis et al., 1992]

Fourteen asphalt test sections near Lawrence, Kansas were evaluated in this study, where the pavement thickness ranged from 3 to 22 in. The radar surveys were calibrated using 73 ground-truth measurements. This study indicates that blind estimates of asphalt thickness were found to be within 10% of actual thicknesses. When questionable core data were removed, the comparison improved to within 7%. When ground truth measurements were used, the accuracy improved to within 5%.

Florida Study [Fernando and Maser, 1992]

The objective of this project was to test and implement a GPR system in Florida by estimating asphalt pavement and aggregate base thicknesses at five test sites and comparing the results to ground-truth measurements. In this study the asphalt pavement thickness varied from 3 to 6 inches, and the aggregate base thickness varied from 8.5" to 12". Blind estimates of asphalt thickness were within 0.5 inches of the actual thicknesses. Correspondingly, the blind estimates of base thickness were within 0.7 inches of core values taken at the test locations. When the results were calibrated with the ground-truth measurements the accuracy improved to 0.2 inches for asphalt thickness and 0.2 inches for the base thickness.

SHRP Study [Maser, 1992b]

The objective of this study was to evaluate the accuracy of GPR for measuring asphalt and base thickness at ten representative test sites located throughout the US, where the asphalt pavement ranged in thickness from 4 to 17 inches and the base thickness ranged from 4 to 14 inches. The results indicate that the blind radar asphalt thickness predictions correlated with the core data with an R-squared of 0.98 and a standard deviation of .78 inches (7.1%). The relative error decreased to 5.1% when the results were calibrated with the ground-truth information.

FWHA Study [Maser, 1992c]

The purpose of this study was to demonstrate and evaluate the pavement layer thickness measurement technology in concrete and composite pavements. This study was carried out in two states, Arkansas and Louisiana. A 1-mile section of concrete pavement and a 1-mile section of composite (concrete with an asphalt overlay) pavement were evaluated in each state. The concrete pavement was 10" thick at each location. The composite sections ranged in thickness from 15 to 20 inches in total thickness. Five ground-truth measurements (coring) per mile were taken in this study. The results of this study indicate that the error in the predicted concrete thickness ranged from 2 to 7%, whereas the error in the predicted composite thickness ranged from 5 to 13%.

Summary

Overall these above studies demonstrate the ability of GPR as a non-destructive test technology for pavement and base layer thickness evaluation. This technology can provide accurate thickness data over continuous sections of highways. The accuracy of thickness calculations are 7.5% for asphalt and concrete pavements, and within 12% for unbound base layers. Furthermore, asphalt layer thicknesses can be calculated for multilayer asphalt systems, and the thickness of individual layers can be calculated down to a minimum of one inch, provided there is an observable signature in the data, i.e., change in material property, across the interface.

2.2.2 Asphalt density

GPR has been demonstrated to be fairly successful in estimating variations in density (equivalently, void content) of asphalt pavements. The basic idea here is that compaction of the pavement reduces the fractional volume of air and increases the relative proportion of the other components (bitumen and aggregate). Since the dielectric value of air (1.0) is substantially lower than that of either bitumen (2.6) or aggregate (6.0), as the asphalt is compacted its dielectric value will increase. A recent study was performed to quantify this dependence [Saarenketo et al., 1996]. A series of laboratory tests was performed on asphalt mixtures over a range in aggregate types, mixture types, bitumen contents and void contents. These tests included 108 measurements in which the void content ranged from 0.02% to 6.5% and the dielectric values ranged from 2.8 to 5.0. These laboratory results were used to construct a mathematical model that relates the dielectric constant of asphalt (ε_a) to its void content (φ):

$$\varphi = 1 - \rho_f = A \exp(B\varepsilon_a) \quad (5)$$

where: φ = void content = fractional volume of air to total volume
ρ_f = fractional density of asphalt = ρ_{emp} / ρ_{max}
ρ_{emp} = emplaced asphalt density
ρ_{max} = maximum asphalt density (at $\varphi = 0$)

The constants A = 272.93 and B = -1.30 were determined through nonlinear regression by fitting Equation (5) to the data measured in the laboratory. The correlation coefficient (R) of this fit was 0.723. The model predicts that as the dielectric value increases from 3.0 to 5.0, the voids content decreases from 5.7% to 0.4%, in a decaying exponential fashion.

Field tests were performed to estimate the void content of asphalt using GPR. This was accomplished by (1) measuring the amplitudes of the reflections from the asphalt surface, (2) calculating the dielectric constant of asphalt using Equation 3, and (3) using Equation 5 to calculate the voids content. These results were compared with those measured in the laboratory. The results of these tests show good correlation (R=0.922) between the predicted (GPR) and measured (laboratory) results.

The implication of these results is significant. Using Equation 5, GPR can be used to estimate fluctuations in asphalt density in a continuous, high-speed, nondestructive fashion, with a fairly high degree of confidence (more than 90 %). These results can inform subcontractors of any pavement sections that fall below density requirements, and they can take immediate steps to rectify such defective sections.

2.2.3 Moisture Content

GPR can be used to estimate the moisture content in the aggregate base layer. Moisture content is the major factor that influences the measured base dielectric constant, since the relative dielectric constant of water is much higher ($\varepsilon_w = 81$) that that of its other constituents, air ($\varepsilon_w = 1$) and dry aggregate ($4 < \varepsilon_s < 8$). High dielectrics are almost certainly attributable to high moisture contents. The dielectric constant of the granular base (ε_b) is assumed to be a function of the volumetric proportions of its constituent values, using a common mixture law called the complex refractive index model [Halabe et al., 1989]:

$$\sqrt{\varepsilon_b} = \sum V_i \sqrt{\varepsilon_i} \qquad (6)$$

$$= n(1-S)\sqrt{\varepsilon_w} + nS\sqrt{\varepsilon_w} + (1-n)\sqrt{\varepsilon_s}$$

where: V_i = fractional volume of the i^{th} component to total volume

ε_i = dielectric constant of i^{th} component

n = porosity = fractional volume of voids (air + water) to total volume

S = degree of saturation = fractional volume of water to total voids

Assuming a specific gravity of 2.65 for the base solids, Equation (6) can be rearranged and the moisture content (M) can be expressed as:

$$M = \{\sqrt{\varepsilon_b} - 1 - (1 - n)(\sqrt{\varepsilon_s} - 1)\} / \{\sqrt{\varepsilon_b} - 1 - (1 - n)(\sqrt{\varepsilon_s} - 22.2)\} \qquad (7)$$

where: M = moisture content = fractional weight of water to total weight.

A field study was performed to estimate moisture content of the base layer using GPR and to compare the results with laboratory measurements [Maser and Scullion, 1992]. GPR was used to

measure the surface amplitudes from the base layer and estimate the base dielectric (ε_b) using Equation 4. Moisture content was calculated using Equation 7, assuming a base solids dielectric of 6 and the measured porosities. Moisture content measurements were made at 21 locations, and compared with the GPR predictions. The comparison was excellent, with a mean-squared error of 1.9% between the measured and predicted values. Thus, GPR can predict moisture levels in base layers with a high level of confidence.

2.2.4 Stripping

Stripping is a moisture-related mechanism that occurs in asphalt pavements in which the bond between the bitumen and the aggregate is broken, leaving an unstable lower-density layer within the asphalt. Stripping may not be visibly apparent since the pathway for moisture is through subsurface cracks that propagate upward from the asphalt-base interface. This mechanism is accelerated by repeated wet and dry cycles, and the final result is total failure of the bond, leaving a weak unstable layer. GPR may be used to detect stripping, in a nondestructive fashion since the reflections from a lower density material will result in a large negative peak in the waveform. The Texas Department of Transportation (TxDOT) has performed several GPR surveys [Saarenkento and Scullion, 1994; Scullion and Rmeili, 1997] to identify sections of asphalt road systems where stripping may be a concern. Where the asphalt layer is homogeneous (no stripping), the GPR waveform will indicate reflections only at the surface and at the asphalt/base interface. If stripping is present, an additional negative peak (indicative of a lower density material) will be observed between the surface and base reflections. It may be possible to estimate the thickness of the stripped sections as well, if the frequency of the antenna is high enough to delineate sublayering. These above mentioned studies surveyed 220 miles of asphalt roads and identified sections of stripping. These results were compared with "ground-truth" measurements in which cores were taken at 1 mile intervals.
The sections identified with the GPR survey matched the coring results, in the cases where stripping was severe. The depth and thickness of the severely stripped sections were "reasonable" in comparison to the actual results. The thickness estimates from homogeneous sections (no stripping) were close (within 10%) to the actual core thicknesses.

2.2.5 Void Detection

The nondestructive mapping of voids under pavements is of interest because of the potential loss of support. Voids develop because of consolidation, subsidence, and erosion of the base material. Generally, voids occur beneath joints where water enters the layer and carries out the fines. In theory air voids and water filled voids are both detectable using GPR because the dielectric constants of both air (1.0) and water (81) are substantially different than most pavement materials (3-10). If the void is air-filled, a large negative peak will appear in the waveform, since the dielectric constant of air is much less than pavement material. Conversely, a large positive peak in the waveform will appear at the surface of a water-filled void, because the dielectric increases substantially at the interface.

Several laboratory studies have been performed to investigate the effects of GPR on voids. Alongi et al.. [1982] used GPR to examine the effects of separation distance between two concrete slabs. For separation distances smaller than 3 inches, the amplitude of the reflected radar wave was observed to increase proportionately. For separation distances ranging from 3 to 6 in, the amplitude remained constant, but the signal increased in width (time). The radar signal split into two separate waveforms for void spacing greater than 6 in, thereby resolving the upper and lower boundaries of the air void. Even though 6 inches was found to be the theoretical limit

for boundary resolution for air voids in this study, these researchers also identified a graphical technique to resolve void sizes as small as crack widths.

Scullion and Saarenketo [1992] used GPR to detect the location of moisture filled voids underlying a concrete pavement. Because the dielectric properties of the concrete were found to be similar to the base, any substantial reflections in the reflected signal were related to the presence of moisture-filled voids. These observations were correlated with ground-truth testing. They were unable, however, to distinguish between water filled voids and saturated layers.

Similar conclusions were reached by Scullion et al. [1992], who used GPR to detect air-filled and water-filled voids beneath a concrete pavement. These researchers were able to identify moisture-filled voids to thicknesses as small as 1/16", but not able to distinguish these voids with saturated layers without the use of ground-truth testing. GPR was demonstrated to detect substantial air-filled voids greater than ½" in thickness.

2.2.6 Vertical Cracks

There has been amount of research to determine if GPR can be used to locate cracks, especially on concrete bridge decks [Maser, 1991; Warhus, 1995; and Momayez et al.., 1994]. Some testing has also been reported on locating subsurface cracks in asphalt road systems [Maser and Scullion, 1992]. Most of these results have not been encouraging, because they were made at highway speeds with only a few traces per meter. This procedure has inadequate resolution to identify vertical cracks, except where the cracks are large or near the surface. However one study, [Saarenketo and Scullion, 1994] was able to identify vertical cracks in an asphalt road system using a high frequency antenna (1.0 GHz) with a very high sampling density (10-20 scans/m). These vertical cracks appear as sharp hyperbolas on GPR scans, and are detectable at depths to 3 m. The location and persistency of these cracks can be used to identify possible mechanisms.

2.2.7 Subsurface Anomalies

GPR has been used successfully to identify subsurface anomalies. The most common applications to highway engineering include locating buried objects, identifying peat deposits, and locating near-surface bedrock deposits. These applications are discussed separately.

Bowders and Koerner [1982] performed a field study to assess the capabilities and limitations of using GPR to detect and locate buried containers of various sizes, depths, material types, and configurations. The results indicate that steel drums are most easily detected and were successfully located to depths of 11 ft using a 120 MHz ground-coupled antenna.. Empty plastic drums cannot be located using GPR, indicating that plastic is transparent to radar. However, if liquid-filled they can be detected with good precision. Closely spaced drums cannot be distinguished at depth.

Saarenkento et al.. [1992] used GPR to estimate the depth and thickness of peat deposits underlying highways in Northern Finland. Because of its high moisture content, the dielectric constant of peat is very high (50-60). Thus, peat deposits are detectable using GPR because of the dielectric contrast with other geotechnical materials. Using a 500 MHz ground-coupled antenna, these researchers were able to identify peat deposits of thicknesses ranging from 1 to 3 m, with an accuracy of 10%.

The depth of the overburden and location of the bedrock can be determined using GPR, providing that the radar signal can penetrate the overburden soil and the depth to the bedrock is relatively shallow. However, identification of the bedrock interface is sometimes difficult, because the dielectric values of the bedrock and the overburden are similar and the reflected signal amplitude from the interface will be very weak, especially at depth. In these cases the interpretation of the radar scans may only be possible only with the aid of other data (i.e., ground-truth measurements, seismic surveys, and/or location of bedrock outcrops). In addition, if the GPR survey is performed in wintertime, near-surface bedrock deposits can be identified since the frost line does not penetrate the bedrock and the bedrock surface is identified by crack reflections, indicating the presence of ice lenses [Saarenketo and Scullion, 1994]

2.2.8 Rutting

Rutting is a localized depression in the wheelpaths of asphalt highways that occurs because of the concentration of loading. There are two possible mechanisms for rutting: (1) compaction of the asphalt pavement layer; and (2) compaction of the base layer. GPR can be used to identify the mechanisms of rutting, and more importantly, identify possible corrective actions. By comparing the layer thicknesses of two GPR surveys (in the wheelpath and in the lane center), one can identify the layer in which the rutting (compaction) has actually occurred [Roddis et al., 1992]. Because of the relatively high accuracy in asphalt and base layer thickness calculations using GPR, differential layer thicknesses of as small as ½" are possible. By monitoring the time-history of the rutting, one can more accurately project the life of the highway, and even identify which layers have been adequately designed or underdesigned.

3. Task 2: Calibration/Sensitivity Studies

3.1. Calibration Studies

A simple laboratory experiment was performed to calculate the dielectric constant of a concrete slab and estimate its using GPR. Three antennas (1000 MHz, 1500 MHz, and 400 MHz) were used in this experiment. The collection characteristics of these antennas are given in Table 3-1.

Table 3-1 Antenna Collection Characteristics

Antenna (MHz)	Type	Range (ns)	Sampling rate (scans/s)
400	Ground coupled	50	64
1000	Air coupled	20	128
1500	Ground coupled	12	100

Two layer configurations were used in this study. Configuration #1 is shown in Figure 3-1. This configuration was used to calculate the velocity of radar in air and to measure the amplitude of the reflected radar signal from a metal surface, necessary for evaluation of the material dielectric of the concrete layer in Configuration #2. In this configuration an 8" piece of styrofoam, which is dielectrically equivalent to air, was used to hold the 1000 MHz air-coupled antenna above a large metal sheet. The GPR results for this configuration are shown in Figure 3-2, which shows the magnitude of the reflected signal (Volts) as a function of time (ns). The measured times of the antenna-end and metal reflections are 2.04 ns and 3.5 ns, respectively. Using Equation 1, the radar velocity is air is calculated to be 11.8 in/ns, which is identical to the theoretical value. Also shown in this figure is the amplitude of the reflected signal from the metal base (A_m = 40,554 V).

Figure 3-1 Configuration #1 Setup – 1000 MHz Antenna

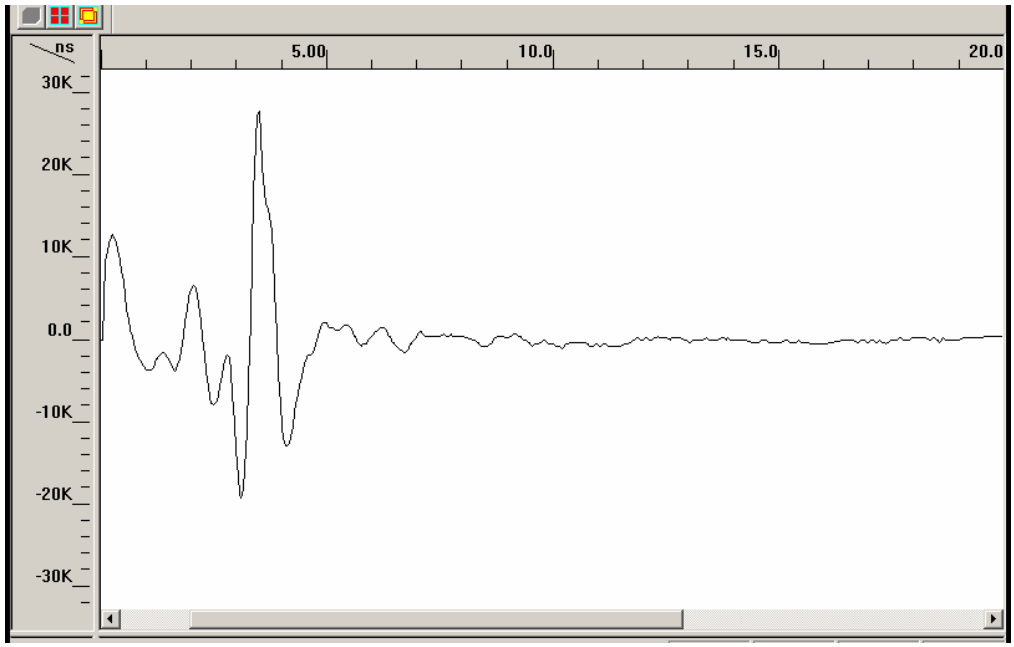

Figure 3-2 Configuration #1 Results – 1000 MHz Antenna

Configuration #2 is shown in Figures 3-3 – 3-5 for the 1000 MHz, 1500 MHz, and 400 MHz antennas, respectively. This configuration was used to estimate the dielectric constant and the thickness of a concrete slab. The slab dimensions are 48" x 48" x 11 ½", which are large enough to give meaningful results. Figure 3.6 shows the reflected results using the air-coupled antenna. As can be seen in this figure, the amplitude of the concrete surface reflection is 22,773 V and the estimated travel time through the layer is 6.57. Using Equation 2, the calculated concrete dielectric constant is 3.562 = 12.68. Similar results are shown in Figures 3-7 and 3-8 for the 1500 MHz and 400 MHz antennas. The estimated travel times through the concrete layers using these antennas are 6.24 and 6.5 ns, respectively. Using Equation 1, the estimated layer thicknesses are 11.0 for the 1000 MHz antenna, 10.3 in for the 1500 MHz antenna, and 10.4 in for the 400 MHz. These results are all within 10% of the actual thickness of 11 ¼", and are in general agreement with those found in the literature for concrete layer evaluations. Future calibration studies should consider the effects of material types, layering, voids, cracks, and moisture.

Figure 3-3 Configuration #2 Setup – 1000 MHz Antenna

Figure 3-4 Configuration #2 Setup – 1500 MHz Antenna

Figure 3-5 Configuration #2 Setup – 400 MHz Antenna

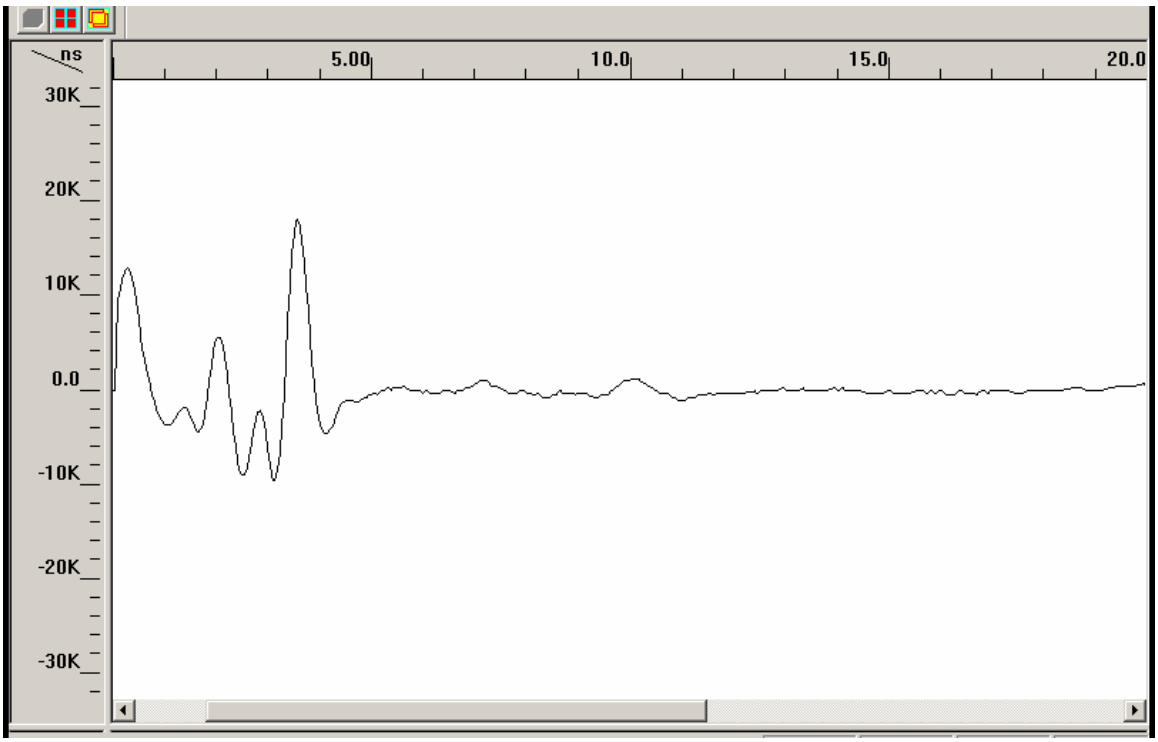

Figure 3-6 Configuration #2 Results – 1000 MHz Antenna

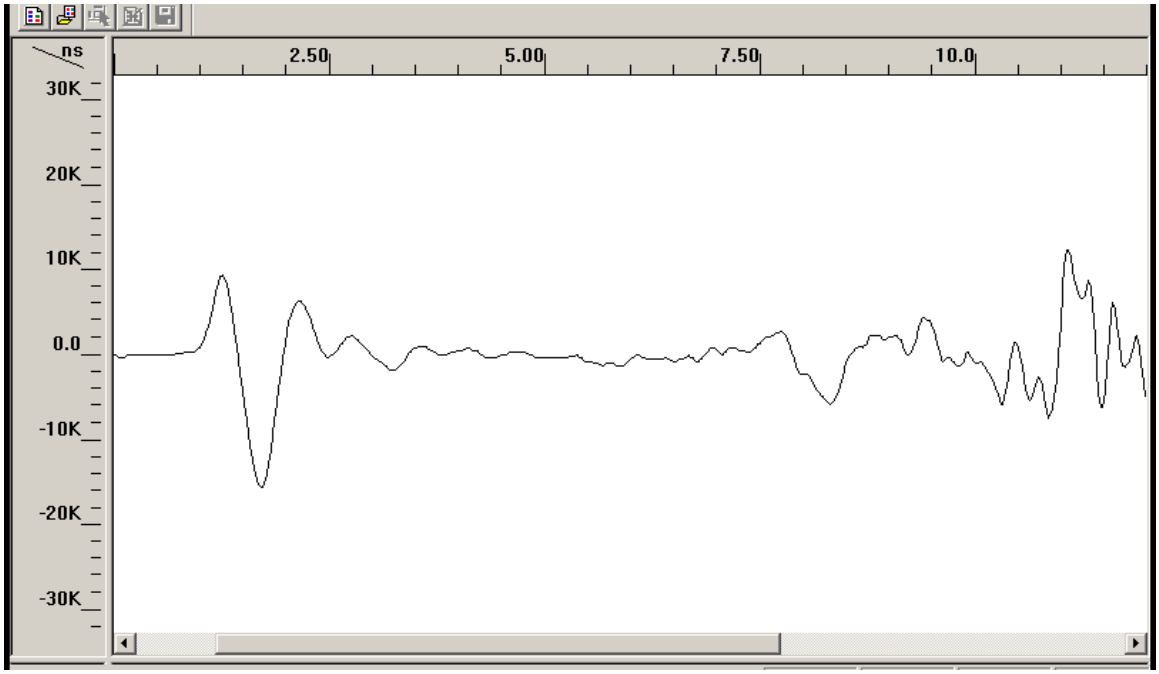

Figure 3-7 Configuration #2 Results – 1500 MHz Antenna

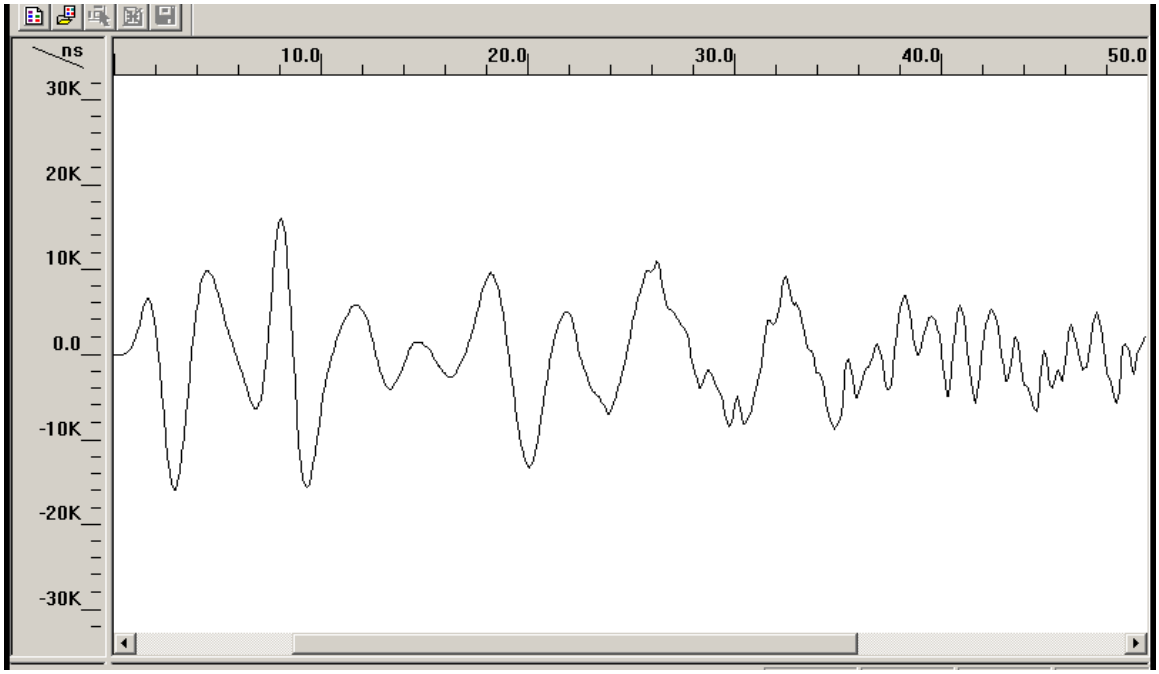

Figure 3-8 Configuration #2 Results – 400 MHz Antenna

3.2 Sensitivity Studies

3.2.1 Vertical Resolution

The minimum layer thickness (d_{min}) that can be resolved using GPR is directly related to the wavelength of the GPR signal (λ);

$$d_{min} = A\,\lambda \tag{8}$$

where A is the fraction of a wavelength necessary to resolve a layer thickness. According to GSSI, the constant A ranges from ¼ to ½, depending on whether the images are computer processed (¼) or not (½). The wavelength is related to the velocity of the medium (v) and frequency of the GPR signal (f) as:

$$\lambda = v/f \tag{9}$$

Finally the velocity is related to the dielectric constant of the medium (γ) as:

$$v = c/\sqrt{\gamma} \tag{10}$$

where c is the speed of light (i.e., the velocity of radar in air) = 0.3 m/ns.

Combining Equations (8) to (10) results in:

$$d_{min} = (Ac) / (f\sqrt{\gamma}) \tag{11}$$

Equation 11 indicates that the minimum resolvable layer thickness is inversely proportional to the antenna frequency and inversely proportional to the square root of the dielectric constant. Table 3-2 gives the recommended vertical resolution of several GSSI antennas in a dry, non-conductive medium ($\gamma = 5$). Equation 8 was fit to this data and A was determined to be 0.275, which falls within the range suggested by GSSI. The comparison between the recommended and predicted (fit) wavelengths is shown in Figure 3.9.

Table 3-2 Vertical Resolution of Various GSSI GPR Antennas

	Vertical
Frequency	**Resolution**
(MHz)	**(m)**
80	0.46
100	0.37
120	0.31
250	0.15
300	0.12
500	0.08
900	0.04

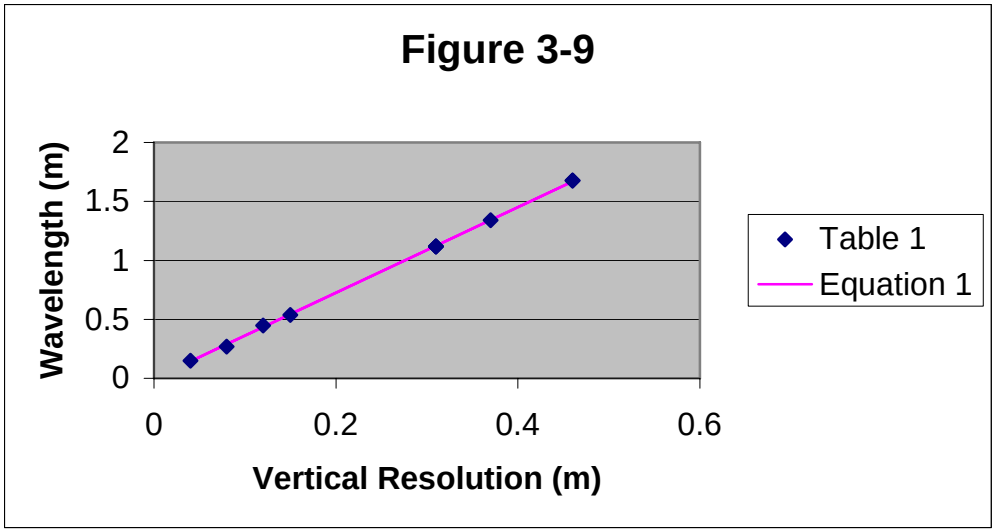

Figure 3-9 Antenna Wavelength as a Function of Vertical Resolution

Table 3-3 gives the vertical resolution for antennas ranging from 100 MHz to 1500 MHz and dielectric constants ranging from 1 (water) to 25 (wet clay). For example, for a 1000 MHz antenna, the vertical resolution decreases from 0.08 m to 0.02 m as the dielectric constant increases from 1 to 16.

Table 3-3 Vertical Resolution (m) for GPR Antenna Frequencies (100 to 1500 MHz) and Dielectric Constants 1 to 25)

	Antenna Frequency (MHz)				
Dielectric Constant (-)		100	400	1000	1500
	1	0.826961	0.20674	0.082696	0.055131
	4	0.413481	0.10337	0.041348	0.027565
	9	0.275654	0.068913	0.027565	0.018377
	16	0.20674	0.051685	0.020674	0.013783
	25	0.165392	0.041348	0.016539	0.011026

3.2.2 Maximum Depth of Penetration

The maximum depth of penetration (D) of a GPR system is dependent on many factors including the radar system (minimum detectable power, total output power, antenna efficiency, antenna gain, and frequency), the medium (velocity and attenuation), and the target (back scatter gain and target cross-sectional area). The frequency of the GPR antenna (f) is inversely proportional to the maximum depth of penetration and exponentially decays with attenuation ($\forall$), viz:

$$f = A \exp(-\forall D)/D^n \qquad (12)$$

where: A and n are constants. Using Equations (9) to (10), Equation (12) can be written as:

$$8 = B \exp(\forall D)\, D^n \qquad (13)$$

Table 3-4 gives the maximum depth of penetration of several GSSI antennas in a dry, non-conductive medium ($\gamma = 5$).

Table 3-4 Maximum Penetration Depths for Various GSSI GPR Antennas

Frequency (MHz)	Depth (m)
80	40
100	30
300	15
400	10
500	6
900	2
1000	1
1500	0.5

Fitting Equation (13) to the data in Table 3-4 results in the following constants:

B = .1146, ∀ = .040, and n = .308. A comparison between the actual and predicted (fit) depths of penetration is shown in Figure 3-10.

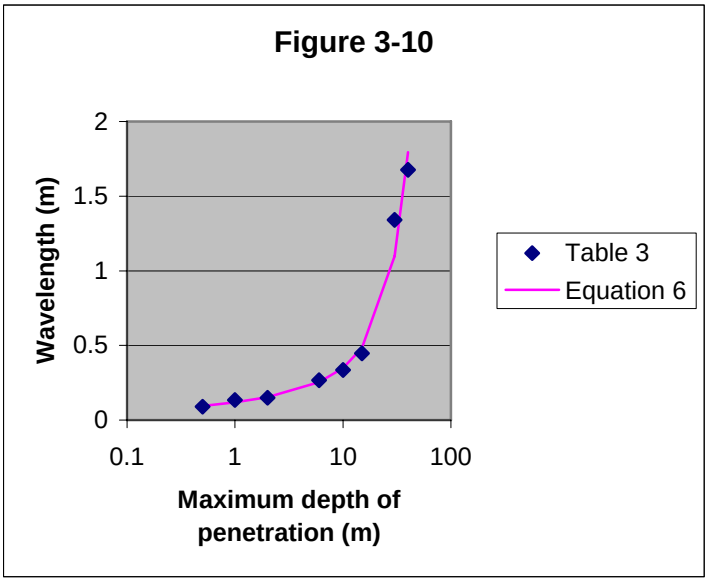

Figure 3-10 Wavelength as a Function of Maximum Depth of Penetration

Table 3-6 gives maximum depths of penetration for various combinations of antenna frequencies and dielectric constants. For example, for a 400 MHz antenna, the maximum depth of penetration decreases from 11.03 m to 3.23 m as the dielectric constant increases from 4 to 16.

Table 3-5 Maximum Depths of Penetration (M) for Various Antenna Frequencies (100 TO 1500 MHz) and Dielectric Constants (1 to 25)

		Antenna Frequency (MHz)			
		100	400	1000	1500
Dielectric Constant (-)	1	50.885	22.7	8.98	3.73
	4	36.29	11.03	1.87	0.59
	9	28.17	5.84	0.59	0.17
	16	22.7	3.23	0.24	0.07
	25	18.66	1.88	0.12	0.03

3.2.3 Horizontal Resolution

GPR antennas emit a cone of radiation. The significant portion of the transmitted energy is reflected to the antenna within a defined circular area beneath the antenna known as the first Fresnel zone. This area increases with depth (d) and wavelength (8). The radius of the Fresnel zone (R_f) can be expressed as:

$$R_f^2 = 8\ d + .25\ 8^2 \qquad (14)$$

The size of the target must be at least 50% of the Fresnel zone to be identified without further processing. Thus, the horizontal resolution can be approximated by the radius of the Fresnel zone. Figure 3-11 is a plot of horizontal resolution as a function of depth for various wavelengths. For example for a 1000 MHz antenna and a material dielectric of 9 (8 = .1), the horizontal resolution increases from .23 m at a depth of ½ m to .32 m at a depth of 1 m.

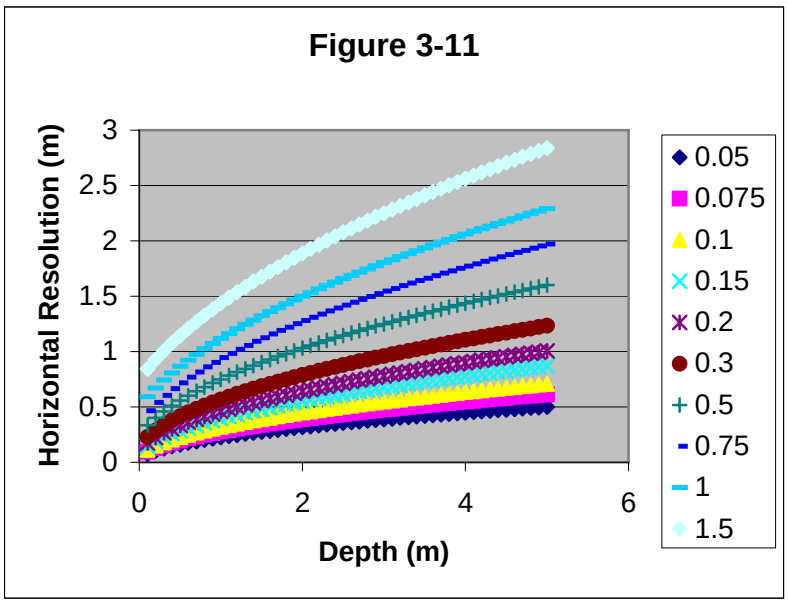

Figure 3-11 Horizontal Resolution as a Function of Depth for Various Wavelengths

3.2.4 Reflection Coefficients

The normal incident reflection coefficient (R) for radar waves on a planar boundary can be expressed as:

$$R = (\sqrt{\gamma_1} - \sqrt{\gamma_2}) / (\sqrt{\gamma_1} + \sqrt{\gamma_2}) \qquad (15)$$

where: γ_1 = Diectric constant of layer 1
γ_2 = Diectric constant of layer 2

where layer 1 overlies layer 2 and R ranges from –1 to +1. When $R < 0$, $\gamma_2 < \gamma_1$ and the peak amplitude of the reflected signal from layer 2 is reversed in sign from layer 1.

When R > 0, $\gamma_2 > \gamma_1$ and the peak amplitudes from both layers are of the same sign. When R=-1, γ_2 approaches zero and layer 2 is a perfect absorber (nothing is reflected). When R=+1, γ_2 approaches infinity and layer 2 is a perfect reflector (metal). Figure 12 shows the relationship between γ_1 and γ_2 for various values of R. From this figure one can classify the reflection coefficients into three general categories, namely; (1) when $*R* < .25$, layer 2 is a weak reflector, (2) when $.25 < *R* < .5$, layer 2 is medium reflector, and (3) when $.5 < *R*< 1.0$, layer 2 is a strong reflector. Thus, the relative strengths of reflections from various layers at a site can be predicted based upon the estimates of dielectric constants. A prior estimate of reflection strengths is useful when determining the optimal data acquisition parameters and when assessing subsurface stratigraphy from the GPR data.

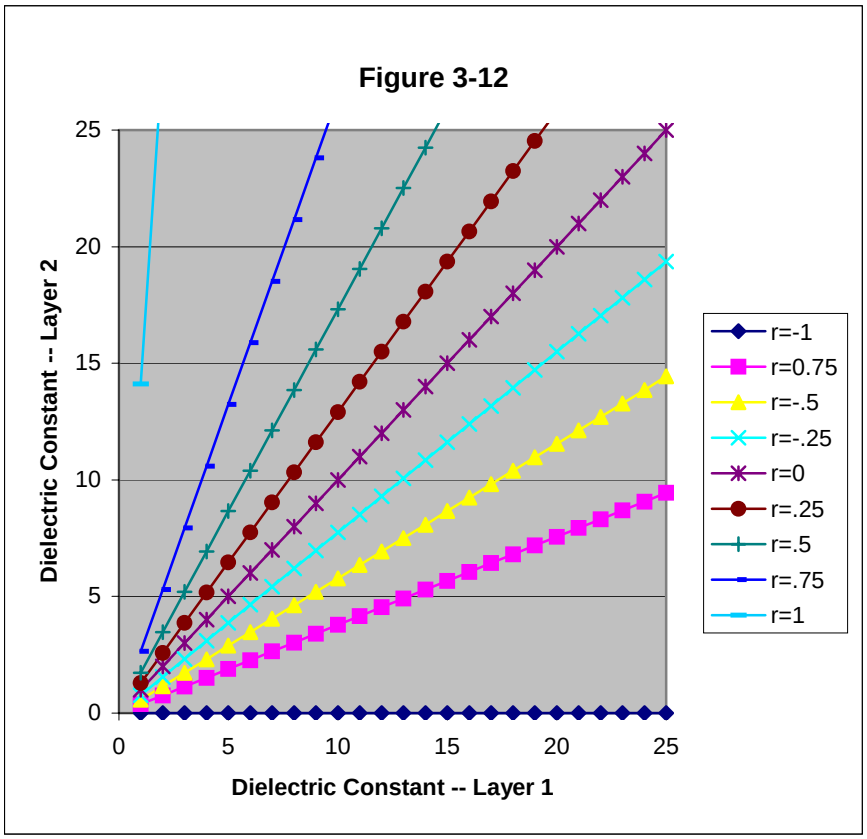

Figure 3-12 Reflection Coefficients for Two-Layer Interface

3.2.5 Layer Thickness

Using the one-dimensional distance equation, the layer thickness (d) can be expressed as:

$$d = \tfrac{1}{2}\, c\, dt/\sqrt{\gamma} \qquad (16)$$

where: c = velocity of radar in air = 11.8 in/ns
dt = travel time across the layer (ns)
γ = dieletric constant of layer (-)

The layer thickness is linearly related to the travel time and inversely proportional to the square root of the dielectric constant (Figure 3-12). This figure can be used to calculate the layer thickness, based on estimate of the material dielectric constant (γ), using the GPR-measured travel times. For example if the measured travel time across a concrete layer (γ=9) is 2.5 ns, the layer thickness is 4.91 ns. This result can also be used to estimate ranges in the calculated layer thickness as well, based on uncertainties in the value of the dielectric constant and variations in the measured travel times. For example, the dielectric constant of the asphalt layer at Cell 34 at the MnROAD site was measured in two different ways, i.e., using a Percometer (γ=4.00) and using GPR calibration with a metal plate (γ=4.50). Analysis of GPR images indicates that the travel time through the asphalt layer in Cell 34 ranges from 1.35 to 1.70 ns, with a mean value of 1.50 ns. Using the mean travel time, the calculated thickness ranges from 4.17 to 4.42 in. The actual thickness (based on construction records) is 4 in. In this case, the GPR estimates are within 10% of the construction based estimates.

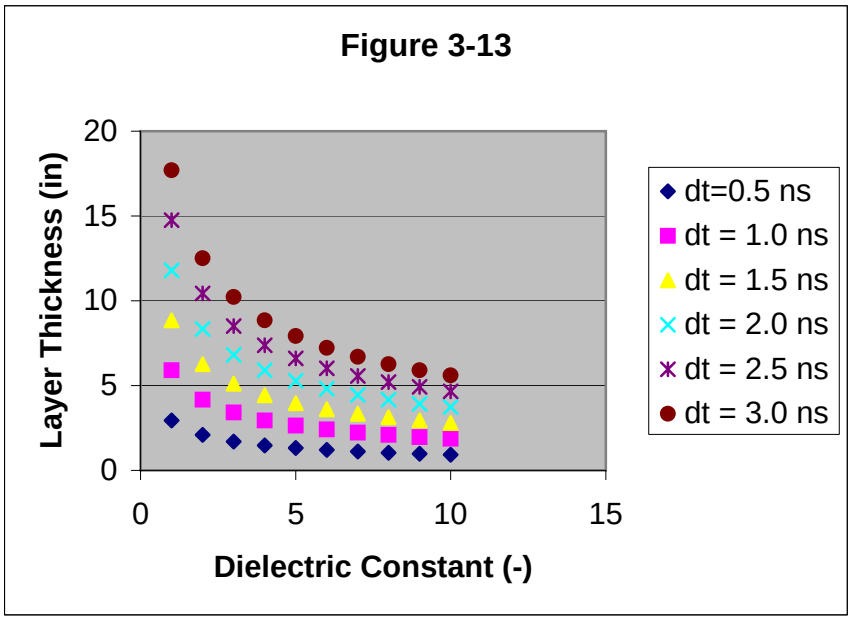

Figure 3-13 Layer Thickness as a Function of Dielectric Constant for Various Travel Times

3.2.6 Air Void Thickness

A laboratory study was performed to determine the sensitivity of two GPR antennas to variations in air void thickness beneath an asphalt slab. Specifically, the objectives were (1) to calculate the air-void thickness using GPR and compare to the actual thickness and (2) to determine the minimum detectable air-void thickness for each antenna. The laboratory setup is shown in Figure 3-14. A 6" asphalt slab is held above a metal plate at a fixed height using Styrofoam, which is dielectrically equivalent to air. The height was varied incrementally from zero to 8 inches. Two antennas were used, a 1000 MHz air-launched antenna and a 1.5 GHz ground-coupled antenna. GPR was used to measure the travel times across the air void for each height and antenna. Equation 16 was used to calculate the thickness, using a dielectric constant of unity for air. The results are shown in Figures 15 and 16 for the 1000 MHz and 1500 MHz antennas,

respectively. For each antenna there is a threshold thickness above which the comparison between the predicted and actual thickness is excellent (R^2 = .99). For the 1.5 GHz antenna this threshold value is 2.0 in (Figure 15) and for the 1.0 GHz antenna this threshold is 3.0 in (Figure 16). These threshold values compare excellently with the theoretical minimum detectable layer thickness for a material with a dielectric constant = 1 (Table 4).

Figure 3-14 Laboratory Setup for Air Void Thickness Study

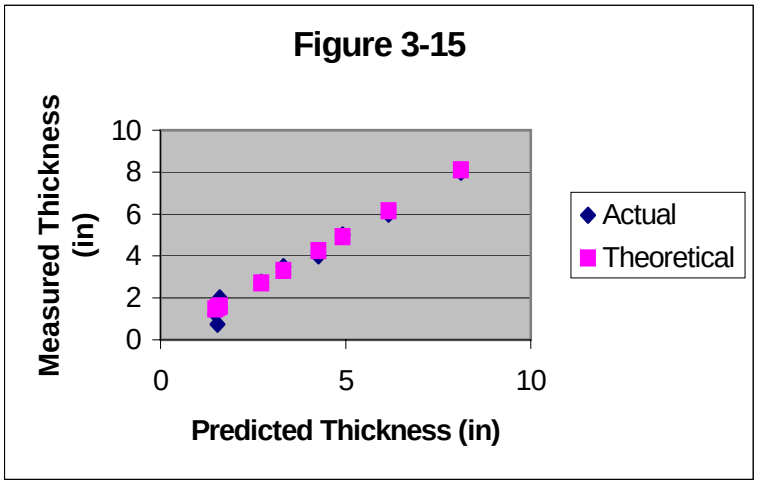

Figure 3-15 Measured and Predicted Air Void Thicknesses for 1.5 GHz Antenna

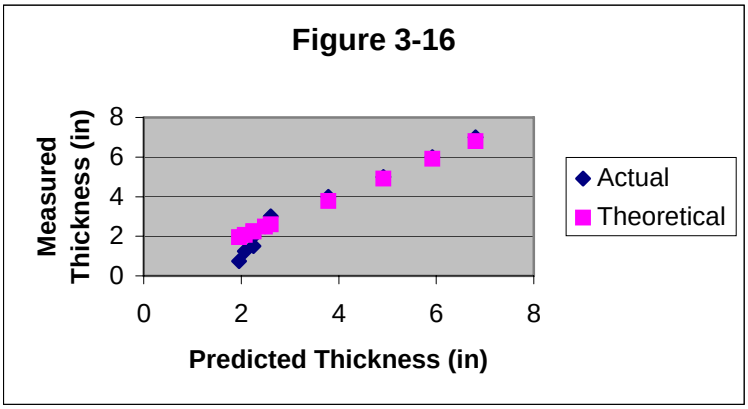

Figure 3-16 Measured and Predicted Air Void Thicknesses for 1000 MHz Antenna

Task 3: CSAH 61 Study

4.1 Site Description

CSAH 61 is a 10.25-mile stretch of highway that runs north from Pine City to the intersection of I-35 (Figure 1). The road begins immediately north of the Snake River Bridge in Pine City (Station 2880+04) and ends at Interstate 35 at Mission Creek (Station 3424+27), a total distance of 54,423 ft. A typical cross-section of the highway is shown in Figure 4-1. According to the original construction plans (Appendix 1) the road consists of four major structural units, (1) asphalt, (2) road mix, (3) aggregate base, and (4) concrete. The asphalt layer is 4 ½" in total thickness, with a 1 ½" wear course and 1" base course, overlying a 2" original asphalt wear course. Two 1" layers of road mix (aggregate base graded in with bitumen) underlie the asphalt layer. A 4-7" layer of aggregate base underlies the road mix. Finally, the aggregate base overlies the original 7-8" concrete roadway.

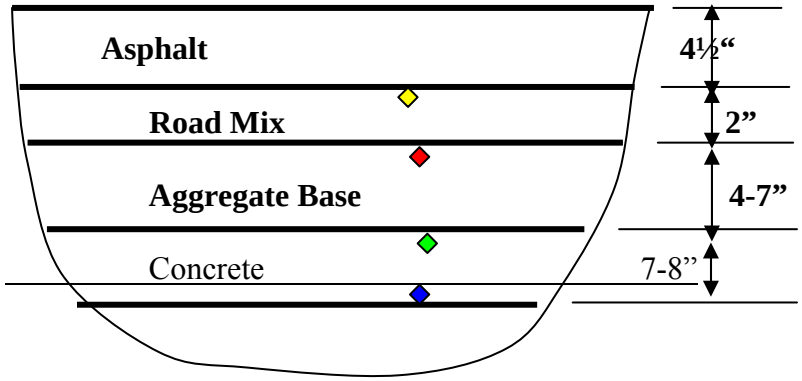

Figure 4-1 Typical Cross-Section of CSAH-61

4.2 Objectives

The objectives of the GPR survey of CSAH 61 in Pine County were (1) to measure the asphalt layer thickness, (2) to estimate the road mix thickness, (3) to detect areas of potential stripping, and (4) to estimate the aggregate base thickness.

4.3 GPR Surveys

Two GPR surveys of CH-61 were performed. The first was performed on September 6, 2002 and the second was performed on October 12, 2003. The first survey was performed in both the northbound (NB) and southbound (SB) lanes at approximately the lane center, and split into smaller, one-mile segments (Table 4-1). The second survey was performed only in the NB lane at approximately the lane center, and split into four segments (Files 001, 002, 003, and 004) of approximately equal length (Table 4-2). In both surveys a 1.0 GHz air-coupled antenna was used, at an approximate vehicle speed of 30 mph. GPR measurements were taken using a 20 ns time window, which allows for layer calculations to an approximate depth of 30 inches. The

sampling density was 3 scans/ft, and an optical encoder was used to coordinate the collection speed with the correct spatial location.

Table 4-1 GPR Survey Markers Along CSAH 61 Pine City to I-35 (Second Survey 9/6/02)

Mile Description	Begin		End	
	ft	Station	ft	Station
1 NB	0	2280+04	5280	2932+84
2 NB	0	2932+84	5280	2985+64
3 NB	0	2985+64	5280	3038+44
4 NB	0	3038+44	5280	3091+24
5 NB	0	3091+24	5280	3144+04
6 NB	0	3144+04	5280	3196+84
7 NB	0	3196+84	5280	3249+64
8 NB	0	3249+64	5280	3302+44
9 NB	0	3302+44	5280	3355+24
10 NB	0	3355+24	6600	3421+24

Table 4-2 GPR Survey Markers along CSAH 61, Pine City to I-35 (Second Survey 10/10/03)

ID #	Marker	Total Distance (ft)	File 001 Location (ft)	File 002 Location (ft)	File 003 Location (ft)	File 004 Location (ft)
1	**Snake River Bridge (N)**	0	0			
2	**(rr) 5th st**	1984	1984			
3	**Airport**	4646	4646			
4	**H 11**	5959	5959			
5	**Grannitt**	11262	11262	0		
6	**Cross Cut**	13958		2696		
7	**19600**	15414		4152		
8	**55 everedy**	19282		8020		
9	**Hilltop**	21882		10620		
10	**Railspur**	24559		13297	0	
11	**h14**	27069			2510	
12	**h 127 (Beroun Ave)**	29374			4815	
13	**130 (Blue ?)**	32343			7784	
14	**Elder**	35038			10479	
15	**Rice**	37634			13075	0
16	**Millard**	42954				5320
17	**30890**	45138				7504
18	**h16 Cross Park**	48533				10899
19	**Tie**	51006				13372
20	**Solid Waste**	51859				14225
21	**I35 Bridge (E)**	54423				16789

4.4 Calibration

The dielectric constant of the asphalt layer was first established, by comparing the magnitude of the reflection from the road surface with the reflection from a metal sheet, using the equation:

$$\varepsilon_1 = \left(\frac{1+\rho_0}{1-\rho_0} \right)^2 \quad (1)$$

where: ε_1 = dielectric constant of first (i.e., asphalt) layer,

$\rho_0 = \frac{A_0}{A_m}$

A_0 = Magnitude of GPR surface reflection from top of asphalt layer

A_m = Magnitude of GPR surface reflection from a metal plate

For the second layer i.e., road mix, the dielectric constant can be calculated in a slightly more complicated fashion:

$$\varepsilon_2 = \varepsilon_1 \left(\frac{1-\rho_0^2+\rho_1}{1-\rho_0^2-\rho_1} \right)^2 \quad (2)$$

where: ε_2 = dielectric constant of second (i.e., road mix) layer,

$\rho_1 = \frac{A_1}{A_m}$

and A_1 = the amplitude of the GPR reflection from the asphalt-road mix interface

Finally, the dielectric constant of the aggregate base (i=3) layer is calculated as:

$$\varepsilon_3 = \varepsilon_2 \left(\frac{1-\rho_0^2+\gamma_1\rho_1+\rho_2}{1-\rho_0^2+\gamma_1\rho_1-\rho_2} \right)^2 \quad (3)$$

where: : ε_3 = dielectric constant of third (i.e., aggregate base) layer,

$\rho_2 = \frac{A_2}{A_m}$

A_2 = the amplitude of the GPR reflection from the road mix-aggregate base interface, and

$$\gamma_1 = \frac{\sqrt{\varepsilon_1}-\sqrt{\varepsilon_2}}{\sqrt{\varepsilon_1}+\sqrt{\varepsilon_2}} \quad (4)$$

Using these equations and the measured results (A_0, A_1, A_2) at selected locations along the GPR survey (See Table below) and comparing them to the metal-plate amplitude (A_m), the dielectric

constants of the three layers were estimated to be approximately 4.3, 10.8, and 11.4. (Note: these amplitudes were not always apparent in all the scans, so appropriate approximations were made) These values are typical of asphalt (4-6) and dry aggregate (8-12) and thus were applied uniformly for these layers, throughout the layer thickness analyses.

Table 4-3 Measured GPR Amplitudes at Selected Locations

Station	⑨$_0$	⑨$_1$	⑨$_2$
2882+54	.32	.09	015
2885+04	.37	.11	.005
2887+54	.40	.09	--
2890+04	.33	.10	.012
2892+54	.38	.12	.008
2895+04	.35	.09	--
Average =	**.35**	**.1**	**.01**

4.5 Material Layer Thickness

The GPR images were analyzed to identify the material layer interfaces and layer thicknesses, using the associated measured travel times through the each of the layers (Δt_i). This was accomplished using the software, RADAN, a computer tool designed specifically for this purpose, that has an automated amplitude-peak search algorithm and subsequently simply measures the time required for the GPR signal to travel across each layer (time of peak amplitude) and return to its surface. The layer thicknesses (d_i) were calculated using the 1-dimensional distance equation:

$$d_i = \frac{c\Delta t_i}{2\sqrt{\varepsilon_i}} \qquad (2)$$

where: c = speed of light (11.8 in/ns)
and ε_i = the dielectric constant of the ith layer.

The travel times were recorded and the information was used to calculate the layer thickness at each point along the survey (where information was visible). The spatial connectedness of these interface points were used to identify the quality of the interface. Because there were no reference drill core data or construction reports available, a "blind" interpretation of the GPR results is presented.

4.6 Results

The results are presented in Appendices 2 and 3, which show a series of dual images of 1000 ft sections along each segment of the GPR survey made during both surveys.

The top image on each page is the visual GPR image, where the horizontal axis is distance along each survey segment (measured in feet) and the vertical axis is time (measured in nanoseconds). The images have been superposed in the horizontal direction and the result is a black and white picture. These colors are used to indicate the magnitude and intensity of the reflected signal. White indicates a positive amplitude reflection (interface); whereas black indicates a negative interface. A white interface is indicative of an increase in dielectric across the interface, and

vice-versa for a black interface. The intensity of the interface indicates the quality or clarity of the interface, i.e., the blacker or whiter the image, the greater is the reflection amplitude and consequently the clearer becomes the interface. The bottom image on each page is the processed image using the automated amplitude peak search algorithm. In these images only the positive peaks are indicated, since in general the lighter negative peaks are a GPR result of the wave approaching and leaving the interface, and not indicative of a true negative interface.

In looking at these figures as the whole, three (and in some instances, four) subsurface interfaces can be clearly identified throughout the survey. Based on construction plans, these three are the asphalt-road mix, the road mix-aggregate base, and the aggregate base-concrete interfaces, respectively. Where visible, the fourth interface represents the concrete base. The GPR characteristics of these four layers are summarized in Table 4-4.

Table 4-4 Layer Types and Characteristics Along TH-61

Layer	Dielectric Constant (-)	Mean Thickness (in)	GPR Base Interface Quality
Asphalt	4.3	4	Excellent
Road Mix	10.8	3	Good
Aggregate Base	11.4	5	Fair
Concrete	12 (Est.)	8	Poor

The top interface (asphalt base) is the most clear and most persistent throughout both surveys. It clearly identifies the asphalt-road mix interface. It occurs throughout the survey at a mean depth of 4"; with some variations at specific locations as well as possible omissions at local interchanges. Identifying sub-layers within the asphalt layer was not possible in this survey, indicating a dielectric similarity in the wearing and base courses. See for example Figure 1 in Appendix 3.1. The base of the asphalt is clearly identified in this section (Station 2880+04 to Station 2890+04) at a depth of approximately 4.5 throughout the section.

The second visible interface (road mix base) is distinguishable for a majority of the survey, although less clear than the asphalt base. The GPR results indicate that the road mix is approximately 3" in thickness where it is apparent; however, there are sections where this layer is vacant, either indicating that the layer is missing, or dielecrically too similar to the overlying (asphalt) and underlying (aggregate base) layers to be distinguishable using GPR. See for example, Figure 1 in Appendix 3.1. The base of the road mix is visible across most of the 1000' section, with a mean thickness at this location of 3"

The third visible interface (aggregate base) is visible in select locations along the survey. These results indicate that this layer has a mean thickness of approximately 5", where it is apparent. For example, the aggregate base is visible at a depth of 9" in Figure 1. In this location, the base thickness is only 4".

Finally, in some rare instances along the survey, the base of the original concrete roadway can be identified. As shown in these figures the concrete is encountered at an approximate depth of 12-14" and has a mean thickness of 8", where it is visible. For example, Figure 4 in Appendix 3.1, the base of the concrete is barely visible at a depth of approximately 14", with an apparent thickness of 7".

Stripping is evidenced by negative reflections in the GPR scans, and/or where the quality of the interface is poor. These results are shown in the figures of the appendices. The results indicate that there may be two sections where the interface quality is poor and stripping may have occurred. The sections where stripping is evidenced is indicated in the summary tables in the appendices. For example, from Station 2940+04 to Station 2950+04 shown in Figure 7 in Appendix 3.1, stripping is evidenced within the asphalt layer as strong oscillations in the GPR signal.

5. Task 4: CSAH 48 Study

5.1 Site Description

CSAH-48 is a 5-mi-long asphalt highway, locally known as La Vaque Rd, located in St. Louis County that connects TH 2 (Station 000+00) in Proctor with TH 53 (Station 264+00) near the Duluth Airport. Generally speaking, under 4-9" of bituminous pavement, the soils the site consist of a 0.7 to 1.5 feet thick layer of Class 5 or silty sand fill (poorly-graded sand) followed by varying amounts of imported silty sand fill to 3.5 feet, all over native silty sand and sandy silt. Layers of organic silt and sandy peat/peat are encountered at several locations, as shallow as 2 ft. In addition, bedrock was also encountered at some near surface locations, as shallow as 2 ft. Note: there are surface expressions of peat and bedrock in the near vicinity of the road.

5.2 Objectives

The objectives of this study are to use GPR to locate near-surface bedrock deposits and/or peat deposits underlying CSAH 48 in St. Louis County and to correlate the results with coring results.

5.3 GPR Surveys

Two GPR surveys of CSAH 48 were performed this year. The first survey was done in April, southbound from the junction of Morris Thomas Rd into the City of Proctor to 6th St, a distance of 14,755 ft (Table 5-1).

Table 5-1 Distance Features Along First GPR Survey of CSAH 48, Southbound from Morris Thomas Rd. to 6th St.

SB Marker	Road or Mail Box Description	Distance (ft)
1	Morris Thomas	0.0
2	Benson Rd.	980.6
3	Wagner	1324.7
4	Hanson	2229.3
5	3615	2762.4
6	Thompson	3265.4
7	3584	3638.4
8	3562	4312.7
9	3554	4610.7
10	Sheridan	5503.3
11	3517	5865.3
12	3509	6093.6
13	3503	6264.3
14	1754	6674.9
15	1740	7018.7
16	Pine	7554.2
17	Johnson	8162.4
18	1641	9119.4
19	St. Louis River	9982.4
20	15th St	11012.2
21	1305	11666.2
22	12th St.	12327.0
23	11th St.	12976.0

24	**9th St.**	**13644.1**
25	**8th St.**	**14020.1**
26	**7th St.**	**14387.8**
27	**6th St.**	**14755.5**

The second survey was done in October of 2003, northbound from the junction of Morris Thomas Rd to the intersection with TH53 near the Duluth Airport, a distance of 10,678 ft (Table 5-2). The objectives of these surveys were (1) to investigate the subsurface beneath the road, primarily to identify near-surface bedrock and/or peat deposits and (2) to correlate these GPR results with field measurements. A 400 MHz antenna with a time window of 50 ns was used in both these surveys. This allows for a penetration depth of approximately 7 ft, using reasonable estimates for dielectric constant. A sampling density of 3 scans/ft and a survey speed of approximately 10 mph were used in both these surveys.

Table 5-2 Distance Features Along Second GPR Survey of CSAH 48, Northbound from Morris Thomas Rd. to TH53

Road or Mail Box Description	NB Marker	Distance (ft)
TH53	**30**	**10678.0**
4089	**29**	**10369.1**
4081	**28**	**10164.8**
4071	**27**	**9941.6**
4061	**26**	**9717.3**
4051	**25**	**9377.5**
4041	**24**	**9124.4**
4039	**23**	**8989.8**
4036	**22**	**8685.9**
4026	**21**	**8611.2**
4017	**20**	**8447.7**
4009	**19**	**8187.6**
3999	**18**	**7989.3**
3976	**17**	**7448.2**
3969	**16**	**7225.0**
3960	**15**	**6943.9**
3953	**14**	**6843.3**
3940	**13**	**6192.5**
3891	**12**	**5123.2**
3886	**11**	**4942.9**
Hermantown	**10**	**2750.5**
3790	**9**	**2452.5**
3785	**8**	**2219.3**
Country	**7**	**1943.3**
3768	**6**	**1810.7**
3750	**5**	**1450.0**
3748	**4**	**1313.4**
3721	**3**	**566.0**
3707	**2**	**223.2**
Morris Thomas	**1**	**0.0**

5.4 Depth Calculation

The GPR images were analyzed to identify the locations and depths to bedrock and /or peat deposits. These depths were calculated, using the associated measured travel times from the surface to the bedrock interface and return to the surface (Δt). This was accomplished using the software, RADAN, a computer tool designed specifically for this purpose, that has an automated amplitude-peak search algorithm and subsequently simply measures the time required for the GPR signal to travel from the road surface through the overlying material, reflect from the bedrock/peat interface, and return to the surface (time of peak amplitude). The depth (d) was calculated using the 1-dimensional distance equation:

$$d = \frac{c\Delta t}{2\sqrt{\varepsilon}} \qquad (1)$$

where: c = speed of light (11.8 in/ns)
and ε = the average dielectric constant of the overlying material

This information was calculated and recorded at each point along the survey (where possible). The spatial connectedness of these interface points were used to identify the quality and depth of the interface.

5.5 Calculation of Average Value Dielectric Constant

Prior to road construction in the late summer of 2003, a detailed soil borings report was published and identifies the subsurface structure on CSAH-48 between Morris Thomas Rd northbound to TH53. Specifically, 59 soil borings were taken which, for the purposes of this report, identify the depth to bedrock at 17 locations, and depth and thickness of peat deposits at 15 locations. (Table 5-3).

Table 5-3 Depths to Bedrock and Peat Deposits along CSAH 48, Morris Thomas Rd to TH53

CSAH 48 Boring #	Descriptive Location	NB Distance (ft)	Station (100 ft)	Elevation (ft)	Peat Top (ft)	Peat Bottom (ft)	Bedrock Top (ft)	GPR Time (ns)
1	Morris Thomas Rd	0	157.62	1326				
2	tb-99-1	148	159.1	1326				
3	b1c	438	162	1334				
4	tb-99-2	788	165.5	1345				
5	b2a	1163	169.25	1356				
6	tb-99-3	1578	173.4	1357				
7	b3a	1778	175.4	1356	4	7		
8	b3b	2088	178.5	1357	3.5	4		
9	b3c	2298	180.6	1357	3.8	6.2		
10	tb-99-4	2388	181.5	1358	3.5	6.5		
11	b4a	2588	183.5	1359	3.5	7		
12	tb-99-5	2873	186.35	1360				
13	tb-99-6	3328	190.9	1349				
14	b6a	3543	193.05	1354				

15	tb-99-7	3788	195.5	1348				
16	tb-99-8	4058	198.2	1340				
17	b8a	4208	199.7	1334				
18	tb-99-9	4313	200.75	1332	4	5.6		
19	b9a	4363	201.25	1331	2	4.5		
20	b9b	4628	203.9	1332			5	17.5
21	tb-99-10	4688	204.5	1333			2.7	8
22	b10a	4688	204.5	1333			3.8	
23	b10b	4728	204.9	1333			6.2	
24	b10c	4798	205.6	1333			5.8	
25	b10d	4898	206.6	1333				
26	tb-99-11	5138	209	1332				
27	b11a	5358	211.2	1329				
28	b11b	5498	212.6	1327	2	3		
29	tb-99-12	5608	213.7	1324			3.6	
30	b12a	5608	213.7	1324			9.7	20
31	b12b	5688	214.5	1322				
32	b12c	5688	214.5	1322				
33	tb-99-13	5768	215.3	1321			2.2	
34	b13a	5768	215.3	1321				
35	b13b	5813	215.75	1320	4	9		
36	tb-99-14	5918	216.8	1320	4	10		
37	tb-99-15	6058	218.2	1321	5	7.3		
38	b15a	6393	221.55	1331			5.3	
39	b15b	6668	224.3	1341			2.2	
40	tb-99-16	6873	226.35	1347				
41	b16a	6973	227.35	1351			10	18
42	b16b	7113	228.75	1355				
43	tb-99-17	7168	229.3	1356			2.6	
44	b17a	7168	229.3	1356			6.4	15.7
45	b17b	7228	229.9	1357				
46	b17c	7463	232.25	1354	4.5	7		
47	tb-99-18	7573	233.35	1351	4.5	7.5		
48	b18a	7683	234.45	1352	4	4.8		
49	b18b	7898	236.6	1359				
50	tb-99-19	7968	237.3	1362			7.3	
51	b19a	8023	237.85	1365			5.7	
52	b19b	8288	240.5	1380			10	
53	b19c	8493	242.55	1389				
54	tb-99-20	8688	244.5	1396				
55	tb-99-21	9323	250.85	1395				
56	b21a	9488	252.5	1392			9	18
57	tb-99-22	10223	259.85	1379	8.3	9.5		
58	b22a	10518	262.8	1387				
59	us 53	10678	264.4	1389				

Also indicated in this table in the last column are the two-way travel times (as recorded by GPR) at the specific locations where the bedrock was visible. Using this information the measured thickness was fit to these recorded times (summarized in Table 5-4), as shown in Figure 1 to

determine the linear correlation between thickness and time. This slope was estimated to be 5.44 ns/in.

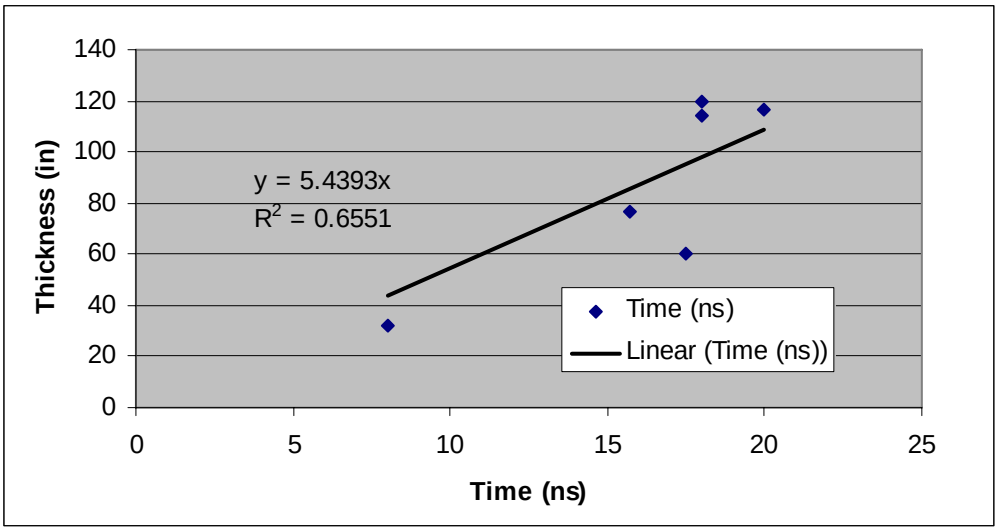

Table 5-4 Depths to Bedrock (Soil Borings) and Two-Way Travel Times to Apparent Interface (GPR)

NB Distance (ft)	Depth (in)	Time (ns)
4628	60	17.5
4688	32.4	8
5608	116.4	20
6973	120	18
7168	76.8	15.7
9488	114	18

Equation (1) was used to evaluate an integrated average dielectric constant. That is,

$$\frac{d}{\Delta t} = \frac{c}{2\sqrt{\varepsilon}} = 5.44 \qquad (2)$$

Thus, the dielectric was calculated to be 1.5, which is realistically impossible, since that would indicate that the material is nearly air. Therefore, a more realistic value of $\bar{\varepsilon} = 8.0$ was assumed throughout this analysis to provide more reasonable results. This value is typical of a volume-averaged mixture of asphalt (ε_a=5), medium-dry aggregate (ε_b=8), and a partially-saturated sub base (ε_s=10), calculated as:

$$\sqrt{\bar{\varepsilon}} = \frac{V_a\sqrt{\varepsilon_a} + V_b\sqrt{\varepsilon_b} + V_s\sqrt{\varepsilon_s}}{V_a + V_b + V_s} \qquad (3)$$

where: V_a = normalized asphalt volume = 7”/42”
V_b = normalized aggregate-base volume = 18”/42”
V_s = normalized sub-grade volume = 17”/42” in the top 3 ½ feet.

5.6 Results

The results are presented in Appendices A and B, which show a series of dual images of 1000 ft sections for each of the two surveys. The top image on each page is the visual GPR image, where the horizontal axis is distance along each survey segment (measured in feet) and the vertical axis is time (measured in nanoseconds). The images have been superposed in the horizontal direction and the result is a black and white picture. These colors are used to indicate the magnitude and intensity of the reflected signal. White indicates a positive amplitude reflection (interface); whereas black indicates a negative interface. A white interface is indicative of an increase in dielectric across the interface, and vice-versa for a black interface. The intensity of the interface indicates the quality or clarity of the interface, i.e., the blacker or whiter the image, the greater is the reflection amplitude and consequently the clearer becomes the interface. The bottom image on each page is the processed image using the automated amplitude peak search algorithm.

A clear subsurface interface is evidenced as a strong reflection in these images, because of the high dielectric contrast between the adjacent materials. Where visible, this interface is indicated in Tables 1 and 2 for each survey. As can be seen in these results, the depth to this interface (where visible) is fairly shallow, consistently between 3 and 4 ft, for example at 1250 ft in the northbound survey (Appendix B).

The GPR images were also analyzed to identify subsurface peat deposits. Peat would appear on the images as a diffused reflection, because of its higher water content. However, none of the images indicated this type of reflection, either because it was out of range of the antenna (greater than 7 ft depth) or the antenna could not detect subtle differences in moisture across the interface, either in the spring or the fall.

6. Summary

GPR is a high-speed, continuous, nondestructive field test that has been demonstrated to give reasonable results in a variety of highway applications, including:

- Based on a comprehensive literature survey,
  - estimating layer thicknesses for asphalt, concrete, base, and subgrade
  - estimating asphalt density
  - estimating moisture content
  - identifying stripping zones
  - detecting subsurface voids
  - locating subsurface anomalies
  - identifying rutting

- identifying parameter sensitivities to antenna frequency and material dielectric, including,
  - minimum layer thickness
  - maximum depth of penetration
  - horizontal resolution
  - reflection coefficients
  - layer thickness
  - air void thickness

- in CSAH 61, GPR was successful at
  - identify the asphalt, road mix, and aggregate base layer thicknesses along a ten-mile stretch of CSAH 61.
  - Asphalt-road mix interface
  - Stripping in isolated zones
  - Concrete base is spot locations

- In CSAH 61, GPR was unsuccessfully at
  - distinguish asphalt lift surfaces (i.e., between base and wearing course) because of the dielectric similarities between the two materials.
- In CSAH 48, GPR identified locations and depths to subsurface interfaces
- In CSAH 48, GPR did not identify near-surface peat deposits, as indicated in soil borings report, because of the presence of a geotextile membrane.

REFERENCES

A. V. Alongi, T. R. Cantor, C. P. Kneeter, and A. Alongi, Jr., "Concrete Evaluation by Radar Theoretical Analysis," *Transportation Research Record* 853, Transportation Research Board, National Research Council, Washington, D.C. (1982) pp. 31-37.

ASTM Standard Designation: D4748-87 *Standard Test Method for Determining the Thickness of Bound Pavement Layers Using Short-Pulse Radar*, American Society for Testing and Materials, Philadelphia, Pennsylvania (1987).

Attoh-Okine, "Using ground penetrating radar as an integral part of the formulation of maintenance decision concerning flexible pavements," *GPR* '94, *Proc. of the Fifth International Conference on Ground Penetrating Radar,* Vol. I of 3, Kitchner, Ontario CA (June 12-16, 1994) pp. 293-303.

L. C. Bomar, W. F. Home, D. R. Brown, and J. L. Smart, *National Cooperative Highway Research Program Re- port 304: Dete1mining Deteriorated Areas in Portland Cement Concrete Pavements Using Radar and Video Imaging,* Transportation Research Board, National Research Council, Washington, D.C. (1988).

J. J. Bowders, Jr., and R. M. Koerner, "Buried Container Detection Using Ground Penetrating Radar," *Journal of Hazardous Materials,* Vol. 7 (1982) pp. 1-17.

O. Buyukozturk, and H. C. Rhim, "Radar imaging of reinforced concrete specimens for nondestructive testing" *Proc. SPIE Nondestructive Evaluation of Aging Bridges and Highways,* Volume 2456 (June 6-7,1995) pp. 186-194.

T. R. Cantor, "Review of Penetrating Radar as Applied to Nondestructive Evaluation of Concrete," ACI Special Publication SP-82 (1984).

C. R. Carter, R. Amorosi, and T. Chung, "An Automated Signal Processing System for the Signature Analysis of Radar

J. L. Davis, J. R. Rossiter, D. Mesher, and C. Dawley, "Quantitative measurement of pavement structures using radar," *GPR* '94, *Proc. of the Fifth International Conference on Ground Penetrating Radar,* Vol. I of 3, Kitchner, Ontario CA (June 12-16, 1994) pp. 319-334.

E. G. Fernando, and T. S. Chua, "Development of a route segmentation procedure using predicted layer thickness from radar measurements," *GPR* '94, *Proc. of the Fifth International Conference on Ground Penetrating Radar,* Vol. 1 of 3, Kitchner, Ontario CA (June 12-16, 1994) pp. 335-349.

E.G. Fernando, K. R. Maser, and B. Dietrich, "Implementation of ground penetrating radar for network-level pavement evaluation in Florida," *GPR* '94*, Proc. of the Fifth International Conference on Ground Penetrating Radar,* Vol. I of 3, Kitchner, Ontario CA (June 12-16, 1994) pp. 351- 365.

C. L. Lau, T. Scullion, and P. Chan, "Using Ground Penetrating Radar Technology for pavement evaluations in Texas, USA," *Fourth International Conference on Ground Penetrating Radar June* 8-13, 1992. *Rovaniemi, Finland,* edited by Pauli Hanninen and Sini Autio, Geological Survey of Finland, Special Paper 16 (1992).pp. 277-284

C. L. Lau, and T. Scullion, "Modeling Ground Penetrating Radar Wave Propagation in Pavement Systems," Research Report 1233-2f, Available through NTIS Texas Department of Transportation (August 1992).

Manitoba Highways and Transportation "Ground Penetrating Radar (GPR) Survey P.T.H. 39, P.T.H. 6 and P. R. 391 Near Thompson, Manitoba." (November 1989).

Manitoba Highways and Transportation "Ground Penetrating Radar Survey of Provincial Trunk Highway Number 1 (PTH) near the Manitoba/Ontario Border 0101-010777" (not dated).

K. Maser, "Bridge Deck Condition Surveys Using Radar: Case Studies of 28 New England Decks," *Transportation Research Record No. 1304,* Transportation Research Board, National Research Council, Washington, D.C. (1991).

K. R. Maser, "Highway speed radar for pavement and bridge deck evaluation," *Fourth 1nternational Conference on Ground Penetrating Radar June* 8-13, 1992. *Rovaniemi, Finland,* edited by Pauli Hanninen and Sini Autio, Geo- logical Survey of Finland, Special Paper 16 (1992) pp. 267-276.

K. R. Maser, "Highway speed radar for pavement thickness evaluation," *GPR* '94, *Proc. of the Fifth International Conference on Ground Penetrating Radar,* Vol. 1 of 3, Kitchner, Ontario, Canada (June 12-16, 1994) pp. 423-431.

K. R. Maser, *Ground Penetrating Radar Surveys to Characterize Pavement Layer Thickness Variations at GPS Sites,* Report No. SHRP-P-397, Strategic Highway Research Program, National Research Council, Washington, D.C. (1994).

K. Maser, and T. Scullion, "Influence of Asphalt Layering and Surface Treatments on Asphalt Base Layer Thickness Computations Using Radar," Report No. TX-92-1923-1, Texas Transportation Institute (September 1992).

K. R. Maser, T. Scullion, W. M. Roddis, and E. Fernando, "Radar for Pavement Thickness Evaluation," *Nondestructive Testing: Second Volume,* ASTM STP 1198 (1994) p. 343-390.

K. R. Maser, "Evaluation of bridge decks and pavements at highway speed using ground-penetrating radar," *Proc. SPIE Nondestructive Evaluation of Aging Bridges and Highways,* Volume 2456 (June 6-7,1995) pp. 237-248.

K. R. Maser, "Evaluation of Ground Penetrating Radar Applications for Pavement and Bridge Management," FHW AI WY-94/01 Wyoming Transportation Department (January 21, 1994)

K. R. Maser, and T. Scullion, "Automated Pavement Subsurface Profiling Using Radar Case Studies of Four Experimental Field Sites," *Transportation Research Record* 1344, Transportation Research Board, National Research Council, Washington, D.C. (1992).

K. R. Maser, *Ground Penetrating Radar Surveys to Characterize Pavement Layer Thickness Variations at GPS Sites,* Report No. SHRP-P-397, Strategic Highway Research Program, National Research Council, Washington, D.C. (1994).

K. R. Maser, "Condition Assessment of Transportation Infrastructure Using Ground Penetrating Radar," *Journal of Infrastructure Systems,* Vol. 2, No.2 (June 1996).

G. R. Olhoeft, "Geophysical detection of hydrocarbon and organic chemical contamination," *Proc. of the Symposium on the Application of Geophysics to Engineering and Environmental Problems, April* 26-29, 1992, Oak- brook, Illinois, edited by R. S. Bell, (April 1992) pp. 587-595.

R. C. Pippert, R. G. Plumb, and Kourosh Soroushian, *Development of a Ground-Penetrating Radar to Detect* Excess *Moisture in Pavement Subgrade,* K-TRAN: KU-91-1, Kansas Department of Transportation (April 1994).

W. M. Roddis, K. R. Master, and A. J. Gisi, "Radar Pavement Thickness Evaluation for Varying Base Conditions," *Transportation Research Record* 1355, Transportation Research Board, National Research Council, Washington, D.C.(1992) pp. 90-98.

T. Saarenketo, K. Hietala, and T. Salmi, "GPR applications in geotechnical investigations of peat for road survey purposes," *Fourth International Conference on Ground Penetrating Radar June* 8-13, 1992. *Rovaniemi, Finland,* edited by Pauli Hanninen and Sini Autio, Geological Survey of Finland, Special Paper 16 (1992) pp. 293-305.

T. Saarenketo, and T. Scullion, "Ground penetrating radar applications on roads and highways," Research Report No. TX-95/1923-2F, Texas Transportation Institute, College Station (November 1994).

T. Saarenketo, and T. Scullion, "Ground penetrating radar applications on roads and highways," Research Report No. TX-95/1923-2F, Texas Transportation Institute, College Station (November 1994).

H. Sihvola, "Self-Consistency Aspects of Dielectric Mixing Theories," *IEEE Trans. Geosci. Remote Sensing,* Vol. GE-27, (1989) pp. 403-415.

T. Scullion, C.L. Lau, and Y. Chen, "Pavement evaluations using ground penetrating radar," *GPR* '94, *Proc. of the Fifth International Conference on Ground Penetrating Radar,* Vol. 1 of 3, Kitchner, Ontario CA (June 12-16, 1994) pp. 449-463.

T. Scullion, C-L. Lau, and Y. Chen, "Implementation of the Texas Ground Penetrating Radar System," Research Report No. FWHAtrX-92/1233-1, Texas Transportation Institute, College Station (Apri11994).

T. Scullion, Y. Chen, and C. L. Lau, "COLORMAP-User's Manual with Case Studies," Report No. FHWA/rX-96/ 1341-1, Texas Department of Transportation (November 1995) p. 90.

S. S. Smith, and T. Scullion, *Development Of Ground- Penetrating Radar Equipment For Detecting Pavement Condition For Preventive Maintenance,* Report No. SHRP- H-672, Strategic Highway Research Program, National Research Council, Washington, D.C. (1993).

P. Ulriksen, "Application of impulse radar to civil engineering," Doctoral Thesis, Lund Institute of Technology, Sweden (1982).